AGU PUBLICATIONS

JGR

Journal of Geophysical Research: Space Physics

RESEARCH ARTICLE
10.1002/2017JA024213

Key Points:
- Westward drift of equatorial plasma bubbles during the 17 March 2015 storm as revealed in airglow imaging observations
- Large westward tilt of equatorial plasma bubbles during the storm
- Asymmetry in the tilt of the plasma bubbles at conjugate points

Correspondence to:
S. Gurubaran,
gurubara@iigs.iigm.res.in

Citation:
Sau, S., V. L. Narayanan, S. Gurubaran, R. N. Ghodpage, and P. T. Patil (2017), First observation of interhemispheric asymmetry in the EPBs during the St. Patrick's Day geomagnetic storm of 2015, *J. Geophys. Res. Space Physics*, *122*, 6679–6688, doi:10.1002/2017JA024213.

Received 31 MAR 2017
Accepted 25 MAY 2017
Published online 10 JUN 2017

First observation of interhemispheric asymmetry in the EPBs during the St. Patrick's Day geomagnetic storm of 2015

Sukanta Sau[1], V. L. Narayanan[2], S. Gurubaran[3], Rupesh N. Ghodpage[4], and P. T. Patil[4]

[1]Equatorial Geophysical Research Laboratory, Indian Institute of Geomagnetism, Tirunelveli, India, [2]National Atmospheric Research Laboratory, Gadanki, India, [3]Indian Institute of Geomagnetism, Navi Mumbai, India, [4]MF Radar Facility, Indian Institute of Geomagnetism, Shivaji University, Kolhapur, India

Abstract In this work, we have studied the characteristics of equatorial plasma bubbles (EPBs), such as their zonal drift and tilt, from the low-latitude and dip equatorial region in the Indian longitude sector during the main phase of the 17 March 2015 storm. All-sky airglow imaging observations from Tirunelveli (8.7°N, 77.8°E geographic, 1.7°N dip latitude) and Kolhapur (16.7°N, 74.3°E geographic, 11.5°N dip latitude) are utilized here. On 17 March 2015, EPBs were observed to drift eastward during 14:30–16:30 UT between 3°S and 15°N dip latitudes. A westward drift presumably under the influence of the disturbance dynamo electric field initially appeared at higher dip latitudes almost 10 h after the storm onset, and subsequently, the same was observed at lower dip latitudes. The EPBs attained a peak westward drift at ~17:00 UT followed by a gradual decrease in their speed till ~18:30 UT. After regaining their westward speed, the EPBs continued to drift westward till 22:00 UT. Moreover, a latitudinal gradient in the drift motion of the EPBs was also observed on this night. Another interesting observation made from the images obtained from Tirunelveli was the presence of a large westward tilt of the EPBs. The most intriguing finding of this study, however, was the asymmetry in the tilt of the EPBs at conjugate points during the premidnight hours on 17 March 2015. In this study, the possible mechanisms that can explain these observations are discussed in light of the current understanding of the equatorial electrodynamics and EPBs.

1. Introduction

One of the most remarkable and commonly observed nighttime phenomena in the low-latitude ionosphere is the equatorial spread *F* (ESF). ESF is a generic name given to represent a class of plasma density depletions with their characteristic alignment along the geomagnetic field lines. Since the first observation of ESF by *Booker and Wells* [1938], a large number of theoretical and experimental studies have been carried out to understand their characteristics and generation mechanism [*Woodman and La Hoz*, 1976; *Zalesak et al*., 1982; *Anderson and Mendillo*, 1983; *Kelley*, 2009; *Narayanan et al*., 2014, and references therein]. Under the action of Rayleigh-Taylor (RT) instability, ESF plumes grow vertically over the dip equator and subsequently map along the field lines to higher geomagnetic latitudes [*Mendillo and Baumgardner*, 1982]. Once they are developed, the irregularities generally drift eastward along with the ambient plasma. The average drift speed and the width of the ESF structures have been reported to be in the range of 50–200 m/s and 50–200 km, respectively [*Rohrbaugh et al*., 1989; *Pimenta et al*., 2003; *Narayanan et al*., 2017]. In the context of optical observations, we refer the plume structures that map along the geomagnetic field lines and extend to higher dip latitudes as equatorial plasma bubbles (EPBs).

One interesting feature associated with the EPBs is their westward tilt. *Woodman and La Hoz* [1976] were the first to report such tilted bubble structures from their analysis of the Jicamarca incoherent scatter radar data. They proposed that an eastward neutral wind blowing through the plume can result in a polarization electric field in such a way that the plume would appear to be drifting eastward at a slower velocity in comparison to the background plasma. Thus, there would be a relative westward drift of the plume which would cause a westward tilt. On the other hand, *Zalesak et al*. [1982] have shown that if a plasma bubble passes through a region where there is already an altitudinal shear in the zonal flow, a westward tilt could be induced in the bubble. *Anderson and Mendillo* [1983] have shown that a latitudinal variation of the zonal wind with a maximum at the dip equator would cause an altitudinal shear in the zonal plasma drift. Subsequently, this shear would induce a westward tilt in the EPBs.

In the past, a few studies have reported on the westward tilt of the plasma bubbles, for example, from radar backscatter [*Woodman and La Hoz*, 1976; *Tsunoda*, 1981] observations, from ground-based optical instruments [*Mendillo and Baumgardner*, 1982; *Mendillo and Tyler*, 1983; *Makela and Kelley*, 2003; *Narayanan et al*., 2017], and from spaceborne optical data [*Kelley et al*., 2003]. From their study using all-sky airglow imaging observations, *Mendillo and Tyler* [1983] found the average westward tilt to be ~0.6° longitude/100 km altitude over the height range of 400–1200 km.

It is known that during quiet geomagnetic conditions, the equatorial ionospheric zonal and vertical electric fields tend to be eastward (westward) and upward (downward), respectively, during daytime (nighttime) [*Fejer*, 1991]. But the low and equatorial ionosphere gets significantly disturbed during a geomagnetic storm. The main sources of these disturbances are the prompt penetration electric field (PPEF) and the disturbance dynamo electric field (DDEF). The reconnection process during the interaction of the solar wind and the magnetosphere induces additional electric fields at high latitudes, which penetrate to the equatorial region through the Earth-ionosphere waveguide [*Nishida*, 1968; *Kikuchi et al*., 1996]. The DDEF is generated when the Joule heating of the high-latitude thermosphere excites a global-scale wind circulation that is opposite to the quiet time tidal wind system driven by solar heating [*Blanc and Richmond*, 1980]. The PPEF is generally short-lived (30 min to 2 h) and is induced almost simultaneously with sudden changes in the *z* component of the interplanetary magnetic field (IMF B_z). On the other hand, the DDEF effects are usually observed 3–4 h after the storm onset and these effects can last a few hours and up to a few days. Generally, during the southward turning of IMF B_z, the induced PPEF would enhance the quiet time electric fields, whereas during northward turning of IMF B_z, the PPEF would impose additional electric field which would be opposite in direction to that during quiet times [*Nishida*, 1968; *Kikuchi et al*., 1996; *Kelley et al*., 1979]. On the other hand, the electric field pattern caused by DDEF would be opposite to that of the quiet time pattern [*Fejer et al*., 1983; *Huang and Chen*, 2008].

On 17 March 2015, the largest storm to date during the current Solar Cycle 24 occurred. This storm caught the attention of larger space science community, and already a number of works have been published describing various aspects of this storm and its manifestations [e.g., *Ramsingh et al*., 2015; *Tulasi Ram et al*., 2016; *Kakad et al*., 2016; *Patra et al*., 2016; *Huang et al*., 2016; *Kil et al*., 2016; *Astafyeva et al*., 2015; *Nava et al*., 2016]. Simultaneous presence of positive and negative ionospheric storms and hemispheric asymmetry in the ionospheric response was observed during this storm [*Astafyeva et al*., 2015; *Carter et al*., 2016; *Nayak et al*., 2016]. *Huang et al*. [2016] showed that the disturbed dynamo effects commenced ~3–4.7 h after the onset of the storm and lasted for almost 31 h. DDEF effects exhibited local time asymmetry during this storm [*Hairston et al*., 2016]. Also, it was pointed out that the PPEF and DDEF effects could have coexisted during this storm [*Tulasi Ram et al*., 2016; *Hairston et al*., 2016]. In addition, *Patra et al*. [2016] showed that the generation of EPBs during this period was confined to a narrow longitudinal region between 69°E and 98°E in the Asian sector.

In this work, we have studied the effects of storm time electrodynamics on the characteristics of EPBs and their evolution in the equatorial and low-latitude region over the Indian longitudes. Using all-sky airglow imaging observations, a comprehensive analysis of the drifts of EPBs at different dip latitudes has been carried out. In particular, the EPBs observed on this night were tilted toward west to a large extent and an analysis of their tilt at conjugate latitudes (3.8°N and 3.8°S dip latitudes) revealed the presence of an asymmetry. To our knowledge, such asymmetry in the plasma bubble appearance at conjugate points has not been reported previously. The results presented in this work are explained in the context of our present knowledge of the equatorial electrodynamics and the nature and occurrence of EPBs during disturbed times.

2. Instruments and Data Analysis

Two all-sky airglow imagers (ASAIs) are being operated continuously from the dip equatorial station, Tirunelveli, and the low-latitude station, Kolhapur, in the same longitude sector during favorable weather conditions. The field of view (FOV) of the ASAIs at the two sites were restricted to ~140° in order to suppress the light noise emanating from the vehicular motions on the nearby roads. At Tirunelveli, the OI 630 nm nightglow images were recorded with an exposure time of 3 min and at a sequential cadence of 12 min and 6 min alternately. At Kolhapur, images were obtained at a fixed cadence of 6.5 min with an exposure time of 2 min. In addition, an on board 2 × 2 binning was applied to the images obtained from Kolhapur. The acquired raw images were unwrapped and projected onto an equidistance grid. With an approximate

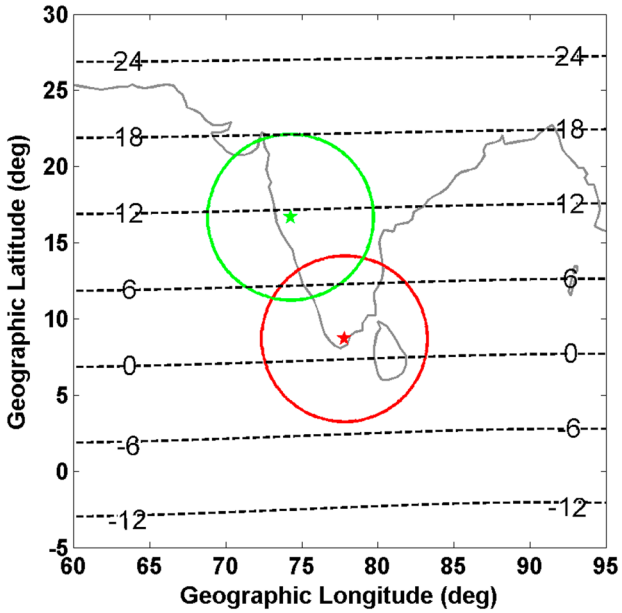

Figure 1. Map showing the locations of the two sites, Tirunelveli and Kolhapur (shown as red and green stars, respectively). The approximate area covered by the ASAI corresponding to a field of view of 140° at an altitude of 250 km is shown separately for the two sites. The black horizontal lines represent magnetic latitudes. The value of the magnetic latitudes has been mentioned on the line itself.

centroid height of ~250 km for the OI 630 nm emission, the FOV of the instrument corresponds to a circular area of ~600 km radius at emission altitudes (Figure 1). The raw images were finally projected over an equidistant grid of 1200 × 1200 km^2 area. A detailed description of the ASAI system and the method of data analysis is available in *Narayanan et al*. [2009].

In this work we begin with estimating the EPB drift velocities at seven different dip latitudes with 3° separation using star removed, projected images over the geographic longitude-latitude grid. The procedure involves extracting individual east-west intensity profiles over a width of 15 km in the north-south direction centered on the chosen dip latitude. An average east-west intensity profile is then estimated by averaging along the 15 km width (i.e., averaging the column of pixels in the 15 km band). From this cross section, we track the troughs or intensity minima which correspond to the EPBs. By identifying the location of the same EPBs in cross sections taken from different images, we estimate the zonal drift velocities. Errors in the estimated drift velocities are usually less than ~12 m/s.

The acquired images are next projected onto the magnetic latitude-longitude coordinate system to calculate the tilt of the EPBs, if any. In this process, for every dip latitude position we consider two locations at ±0.2° latitudes away from it. We then estimate average east-west intensity profiles centered over these two locations using the same method applied to drift calculation. Following this, the zonal shift of the intensity trough corresponding to a particular plasma bubble is taken note of from these two intensity profiles to estimate the tilt. The tilt value thus estimated will have the unit of degree of magnetic longitude per degree of magnetic latitude, which will be henceforth mentioned as degrees longitude/degrees latitude. The error in the tilt value is estimated to be ~ ±0.05° longitude/latitude.

The IMF B_z data of the Wind satellite at 1 min time resolution, time shifted to the nose of the bow shock, were obtained from Space Physics Data Facility (SPDF) of NASA at http://omniweb.gsfc.nasa.gov/form/sc_merge_min1.html. The 1 min data of *SYM-H*, *AU*, and *AL* indices and the hourly-averaged values of *Ap* index were taken from SPDF sites at http://omniweb.gsfc.nasa.gov/form/omni_min.html and http://omniweb.gsfc.nasa.gov/form/dx1.html, respectively. It may be recalled that the *SYM-H* index represents the disturbance in the horizontal component of the magnetic field at midlatitudes due to magnetospheric ring current. The *AU* and *AL* indices are generally used to indicate the presence of magnetospheric substorms, while the *Ap* index represents the level of geomagnetic activity.

3. Results

A solar eruption on 15 March 2015 launched a coronal mass ejection (CME) into space. The CME interacted with the Earth's magnetosphere at ~04:30 UT (UT = Indian Standard Time − 5.5 h) on 17 March 2015, and as a result of the impact, the IMF B_z increased up to 24 nT in the northward direction. Following this, the symmetrical ring current (*SYM-H*) index was increased to 67 nT indicating the onset of storm sudden commencement (see Figure 2). Around 06:00 UT, the IMF B_z suddenly turned southward and simultaneously a storm main phase was initiated. Few northward turnings were observed in the IMF B_z between 06:40 UT and

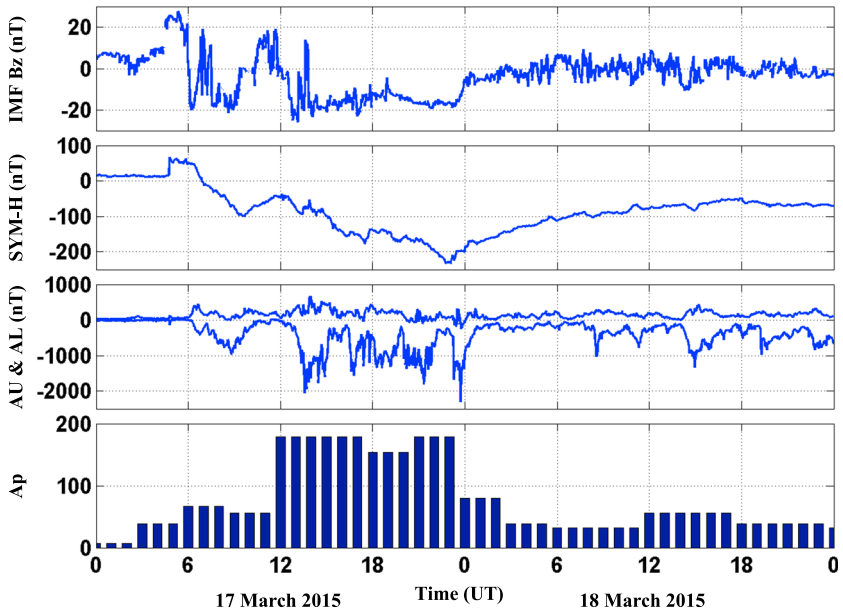

Figure 2. Magnetic activity indices ((first panel) IMF B_z, (second panel) *SYM-H*, (third panel) *AU* and *AL*, and (fourth panel) *Ap*) for the period commencing at 00:00 UT on 17 March 2015 till 24:00 UT on 18 March 2015.

13:50 UT, and later the IMF B_z remained southward for a prolonged period (~12.5 h). The *SYM-H* index on this day decreased initially to −101 nT at 09:37 UT and then started increasing to reach a value of −38 nT at 12:06 UT. The IMF B_z was mostly northward during this period, which is referred to as a temporary recovery period [*Huang et al*., 2016]. After 12:06 UT, the *SYM-H* decreased steadily and attained a peak value of −234 nT at 22:47 UT, making this storm the strongest during the Solar Cycle 24 (refer to Figure 2). The *Ap* index registered a maximum value of 179 during this storm. The *AU* and *AL* indices indicate the presence of several substorms during the main phase as well as during the recovery phase of the storm. At 23:00 UT on 17 March 2015, a gradual recovery of the storm commenced.

The acquisition of the imager data on 17 March 2015 at Kolhapur commenced at 14:00 UT, while at Tirunelveli the same commenced at 14:40 UT. EPBs first appeared in the Kolhapur images over ~15.5°N dip latitude at 14:18 UT. However, at Tirunelveli, EPBs were first observed over ~8°N dip latitude at 15:17 UT. Within a time span of ~30 min, EPBs appeared over the whole FOV of the Tirunelveli imager. A similar observation of EPBs appearing first over higher latitudes and then extending equatorward has been reported by *Rajesh et al*. [2010] using all-sky airglow images obtained over the Indian longitudes. This feature is attributed to the descent of the ionosphere over the magnetic equator into the airglow emission region occurring at later times compared to the descent of the ionosphere at low latitudes occurring at earlier times.

We show a few sets of combined images in Figure 3, which were obtained by stitching together images obtained from Kolhapur and Tirunelveli at similar times. A maximum time gap of 2 min between individual Kolhapur and Tirunelveli images was allowed to stitch them together. The part of the Kolhapur images corresponding to the southern sky and the part of the Tirunelveli images corresponding to the northern sky have been cropped so as to enable us to visualize the continuity in the EPB mapping from lower dip to higher dip latitudes. The presence of clouds affected the image quality between 17:24 UT and 19:06 UT at Tirunelveli. Clouds occurred over Kolhapur between 15:45 UT and 18:10 UT and between 22:15 and 23:30 UT (Figure 3). It was not possible to derive simultaneous drift velocities at all dip latitudes during these times, but still some interesting inferences could be obtained.

As a next exercise, the drifts computed for the prominent EPBs separately within the FOV for any dip latitude sector at a particular time are considered and are averaged to obtain an average drift value at that time. In Figure 4 we show the temporal variation of the average plasma drifts for different dip latitude sectors. Between 14:30 UT and 15:30 UT on 17 March 2015, an eastward drift with speeds in the range of 40–70 m/s was observed at 15°N dip latitude. During the same time period, the magnitude of the

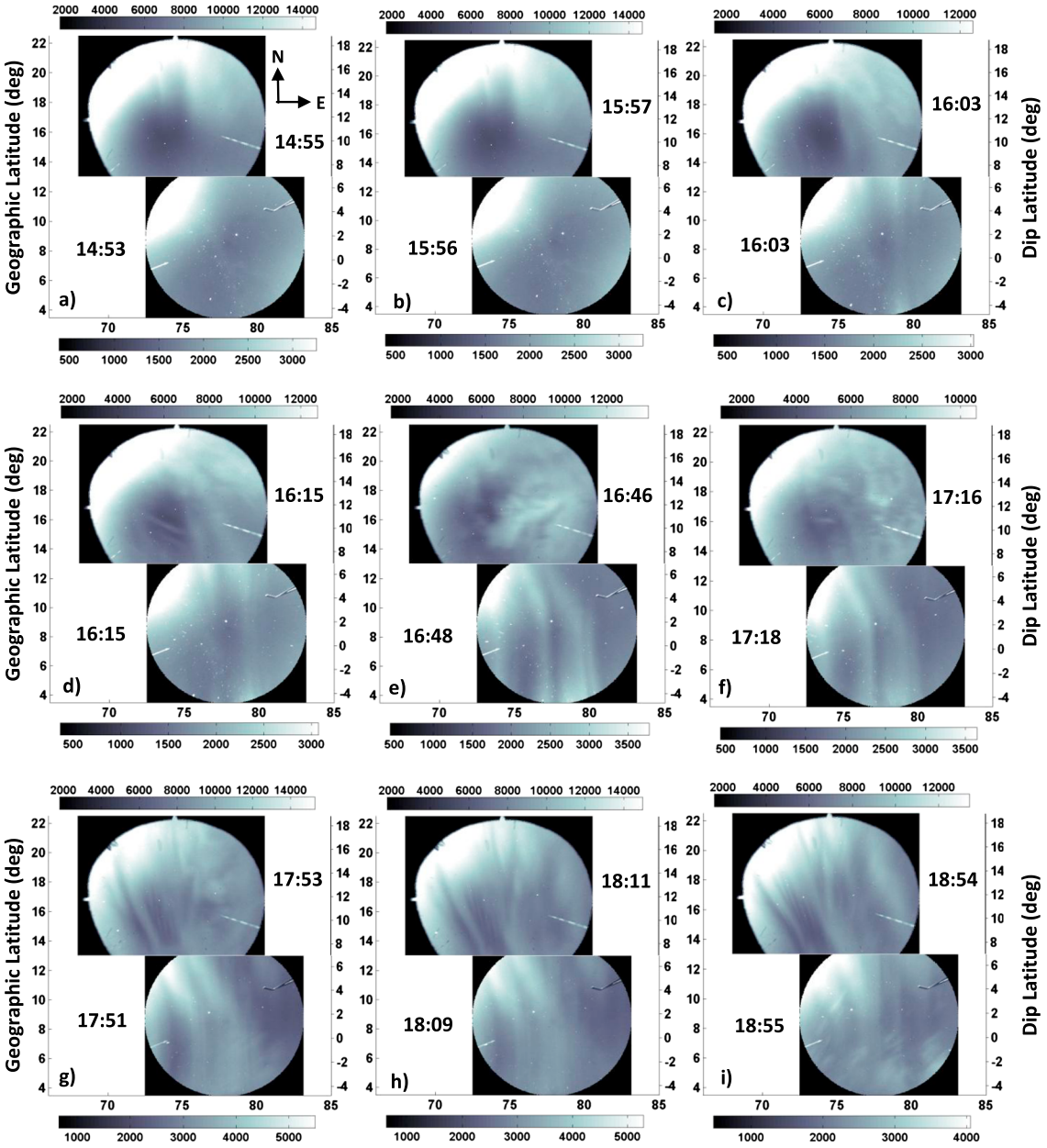

Figure 3. Combined plots of Kolhapur and Tirunelveli images in geographic latitude versus longitude plane. For each pair of images, the Kolhapur images are shown on the top while Tirunelveli images are shown in the bottom. The intensity range in arbitrary units for the Kolhapur images is shown above the combined plots, while for Tirunelveli images it is shown below the combined plots. Dip latitude values along the longitude of Kolhapur and Tirunelveli are shown at the right side of the combined images. Times shown are in UT.

eastward drift was very small at 12°N dip latitude in comparison to 15°N dip latitude. Unfortunately, as mentioned earlier, we do not have information about the drifts between 15:40 UT and 17:50 UT and over the dip latitude sectors between 12°N and 15°N due to the presence of clouds over Kolhapur sky. For this reason, we were unable to determine the actual timing of the eastward drift motion turning westward, especially over the northern dip latitudes of 12°–15°.

From the drift values depicted in Figure 4, it is evident that the EPBs exhibited a change from eastward to westward motion at 9°N dip latitude at 16:10 UT and 6°N at 16:18 UT, respectively. In the region between 3°N and 3°S dip latitudes, the eastward to westward drift reversal was observed later at 16:40 UT. By examining the pattern of the drift reversal at different dip latitudes, it becomes evident that the westward drift of the

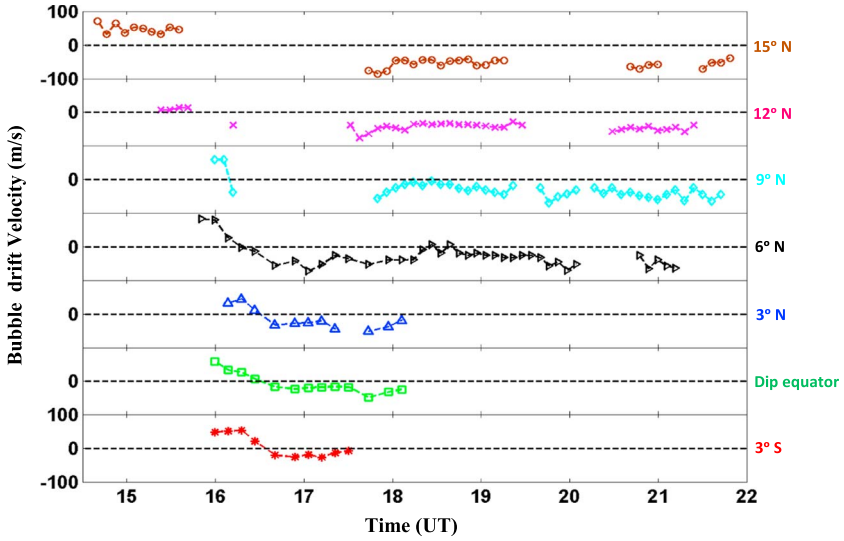

Figure 4. Temporal variation of the bubble drift velocities at different dip latitudes on 17 March 2015. The vertical axis of each panel runs from −100 m/s to +100 m/s. The full vertical axis limit is shown for the top and bottom panels only. For the rest of the panels, only the zero drift line is shown. Dip latitude values in the corresponding line colors are marked on the right-hand side of the figure.

plasma bubbles appeared earlier at higher dip latitudes and subsequently it appeared at lower dip latitudes at later times. The westward drift is seen to peak at ~17:00 UT in the 3°S–6°N dip latitude sectors.

After 17:00 UT, the westward drift velocity gradually decreased in magnitude till ~18:30 UT and subsequently the westward drift increased again. This gradual decrease and subsequent increase of westward drift were observed at almost all dip latitude sectors shown in Figure 4, but it was most apparent at 6°N and 9°N dip latitudes. It is noticed that the EPBs continued to drift westward with velocities in the range of 30–70 m/s till 22 UT (i.e., early morning hours of the next day in the Indian longitude sector) on 17 March 2015. On the other hand, simultaneous occurrence of different drift velocities at different dip latitudes was noticed on this day. Similar latitudinal variations of zonal drift have been reported by a few workers [e.g., *Pimenta et al*., 2003; *Martinis et al*., 2003; *Chapagain et al*., 2011]. While a westward drift was first observed at 9°N dip latitude sector, the presence of eastward drift was noticed at 6°N dip latitude and even for 20 more min eastward drift persisted in the 3°N-dip equator-3°S dip latitude sectors. Again, the magnitude of the westward drift at 6°N was larger than the drifts observed later between 3°S and 3°N dip latitude sectors between 16:30 UT and 18:00 UT. It can be appreciated that such latitudinal gradient in the drift velocity could enforce an apparent tilt on the plasma bubble structure.

We indeed notice the presence of large westward tilted EPBs on 17 March 2015 over the two observing sites. At first, a perceptible signature of westward tilt appeared at 10.5°N–14°N dip latitudes between 16:02 UT and 16:14 UT (Figures 3c and 3d). It can be noted from Figure 3 that the clouds obscured observations at higher dip latitudes during this time. Subsequently, the bubbles at lower dip latitudes started exhibiting westward tilt. In images obtained from Tirunelveli, increasing westward tilt of the plasma bubbles was noticed near 7°N–8°N dip latitude after 16:15 UT. After a time interval of ~30 min, a large westward tilt was observed northward of 3.4°N dip latitude (Figures 3e–3i). The westward tilt attained a peak value of −0.572° longitude/latitude at 6°N dip latitude at ~18:35 UT. Here negative (positive) tilt values represent westward (eastward) tilt of the EPBs.

To verify whether plasma bubbles with such large tilt were present on other days, we examined airglow data from Tirunelveli for an extended period of January to May 2015 (which covers the St. Patrick's storm period). We have chosen 6°N dip latitude as the location to calculate the maximum tilt value on a particular day because beyond this latitude the east-west extent of the image area decreases drastically. Also, a large area of the Tirunelveli images corresponding to northwest part of the sky was under the influence of vehicular light noise, which further restricted the effective area of airglow data northward of 6°N dip latitude. In total

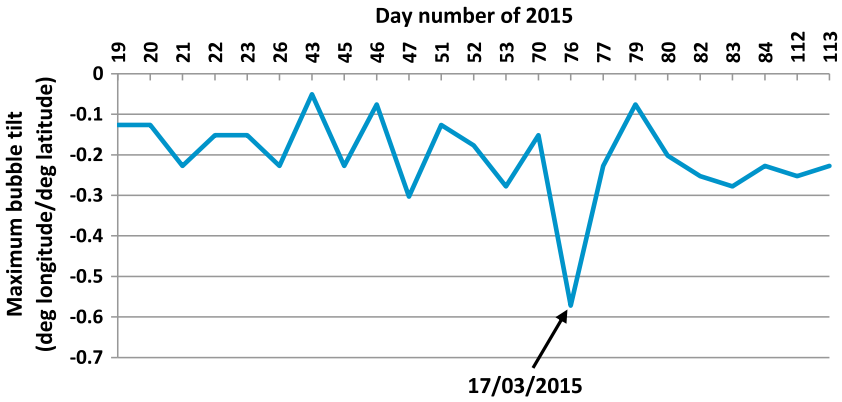

Figure 5. Plot of maximum bubble tilt values observed on a particular day with respect to the corresponding day number during the year 2015. Here tilt values have been estimated with respect to the geomagnetic north.

there were 35 nights of airglow data available during January to May 2015. EPBs were observed on 23 nights. In Figure 5, we present the results for the maximum tilt values of the bubbles observed every night versus day number. As can be seen, on almost 75% cases (17 days) analyzed during the considered period, the maximum tilt value was in the range of 0° to −0.23° longitude/latitude. Maximum tilt values in the range of −0.24° to −0.3° longitude/latitude were observed on 22% cases (5 days), whereas the maximum tilt of the plasma bubbles (−0.572° longitude/latitude) estimated for 17 March 2015 was almost 2 to 10 times larger compared to all other days during the considered period.

Another unique characteristic of the EPBs observed on 17 March 2015 was their asymmetry in the westward tilt at conjugate points. To quantify this asymmetry, we had determined the tilt values at 3.8°N and 3.8°S dip latitude on 17 March 2015. For comparison, we use the tilt values calculated for two quiet days, 22 February 2015 and 22 April 2015. The reasons for choosing these dip latitudes are as follows. First, the large westward tilt on 17 March 2015 mapped till ~3.4°N dip latitude. Second, the EW coverage area of the Tirunelveli imager beyond 4°S dip latitude decreases sharply.

We show in Figure 6 the tilts observed at various times for the 3 days considered herein. On the two quiet nights of 22 February 2015 and 22 April 2015, the observed tilt values at the conjugate points were comparable and/or the deviation between them was within the error limit. Most of the tilt values were confined within the limit of ±0.1° longitude/latitude on the two quiet days. On 17 March 2015, however, tilt values larger than 0.2° longitude/latitude were observed at 3.8°N dip latitude after 16:33 UT, while the tilt at 3.8°S dip

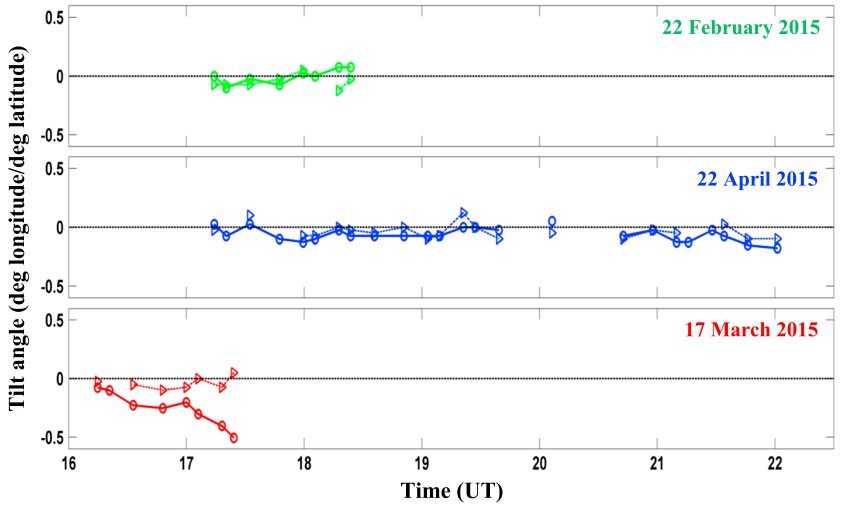

Figure 6. Time variation of tilt at two conjugate points (3.8°N and 3.8°S dip latitude) for 3 days. Continuous and dashed lines represent tilt at 3.8°N and 3.8°S dip latitudes, respectively.

latitude was restricted to within the limit of ±0.1° longitude/latitude. The asymmetry in the tilt increased with time on 17 March 2015. A large difference of ~0.5° longitude/latitude in the tilt values between the conjugate points was observed at 17:24 UT on 17 March 2015. As noted earlier, tilt values could not be estimated at both conjugate points after 17:24 UT due to the presence of clouds. To our knowledge, such interhemispheric asymmetry in the tilt of EPBs at conjugate points has not been reported in the literature previously.

4. Discussion

On 17 March 2015, the airglow observations at Tirunelveli and Kolhapur commenced ~8–9 h after the onset of the storm main phase. Considering this time interval, it was likely that the disturbance dynamo effects had already set in. But it was noticed that EPBs drifted eastward till premidnight hours at different dip latitudes between 3°S and 15°N. Though the presence of clouds made it difficult to determine the exact westward drift reversal time over the 12°N–15°N dip latitude sectors, an apparent westward drift was indeed observed at 9°N dip latitude almost ~10 h after the onset of storm main phase. Also, the drift pattern in Figure 4 indicates that the disturbance dynamo effects appeared first at relatively higher dip latitudes and then traveled toward the dip equator.

The signature of DDEF has been reported at similar times in the Indian longitude sector by other researchers [*Kakad et al*., 2016, *Hairston et al*., 2016, *Patra et al*., 2016]. Also, *Ramsingh et al*. [2015] and subsequently *Tulasi Ram et al*. [2016] reported the presence of strong PPEF over the Indian longitudes during evening hours (~14 UT). Our observation supports the suggestion of *Tulasi Ram et al*. [2016] that DDEF and PPEF might have coexisted in the Indian longitude sector during the premidnight hours. Such a mixed effect of PPEF and DDEF has been observed during this storm at different latitudes of the American sector as well [*Nayak et al*., 2016]. It is plausible that the DDEF effects were masked by the PPEF effects till 15:30 UT, whereas during later hours the electrodynamics were predominantly controlled by the DDEF.

We have already mentioned that there was a gradual decrease in the magnitude of the westward drift between 17:00 UT and 18:30 UT, and subsequently, it increased again. This gradual decrease of the westward drift could be related to the temporary recovery period of *SYM-H* as has been pointed out by *Huang et al*. [2016]. On 17 March 2015, three moderate substorms were observed between 16:20 UT and 18 UT. We do not yet know whether these substorms had any effect on the decrease of the westward drift as we do not have any other supporting information.

The large westward tilt (−0.3° to −0.57° longitude/latitude) close to the dip equator observed in this work has not been reported previously. *Sekar et al*. [2012] noticed simultaneous presence of tilt in plasma bubble structures and shear in the zonal plasma drift in the bottomside *F* region during a disturbed period from the low-latitude station, Gadanki.

Among the days considered for the period January–May 2015, the largest westward tilt of the plasma bubbles on 17 March 2015 was a few times greater compared to that on other days during this period. The large westward tilt on 17 March 2015 mapped up to ~3.4°N dip latitude, which corresponds to an apex altitude of ~270 km. Such a large tilt of the plasma bubbles mapping to apex altitudes as low as ~270 km is a rare feature. The digital range-time-intensity maps shown by *Woodman and La Hoz* [1976] revealed that the base of the tilt structures were located mostly at or above 300 km. Therefore, such large bubble tilt is not generally expected to map so close to the dip equator on quiet days, though *Woodman and La Hoz* [1976] had mentioned that there is a day-to-day variability in the base height of the tilt structure. Our results also support the recently reported observation of *Narayanan et al*. [2017] wherein the tilt of the EPBs was found to be larger during disturbed conditions in comparison to the quiet periods, though the periods considered in their study were weak to moderately disturbed.

We have already shown that a strong shear in the plasma bubble drift velocity was present on 17 March 2015. Moreover, it can be observed from Figure 4 that eastward drifts of considerable magnitude became westward within a small time interval of ~30–40 min. Reversal of plasma bubble drift over such a short duration during this storm was reported by *Patra et al*. [2016] as well. On the other hand, the large westward tilt of the bubbles occurred almost simultaneously with the reversal of the plasma drift velocity. Considering all these aspects, we propose that the large shear in the plasma drifts generated over a short period of time was the possible cause of the large westward tilt.

An intriguing finding of this study is the asymmetry in the tilt of the bubbles at conjugate points within the Tirunelveli imager FOV on 17 March 2015. Such asymmetry was not observed on two other quiet days analyzed in this work (Figure 6). From observations at conjugate magnetic dip latitudes (~ ±24°), *Otsuka et al*. [2002] have shown that plasma bubble structures of 40–200 km EW scale size are identical at these two locations. The cause of this symmetry in the bubble structures between conjugate points is the polarization electric field generated within the bubble. This polarization electric field maps along the field lines to both hemispheres simultaneously from the dip equator [*Mendillo* and *Baumgardner*, 1982, *Kelley*, 2009, and references therein]. When there is a latitudinal gradient in the zonal drift, a deviation of the EPBs from its close alignment to field lines [*Martinis and Mendillo*, 2007, and references therein] is expected to occur. On 17 March 2015, the zonal plasma drifts at 3°N and 3°S dip latitudes were comparable between 16:30 UT and 17:24 UT (Figure 4). The exact reason for the occurrence of such asymmetric tilts at conjugate points is not known. One possibility is that the polarization electric field within the bubbles would have decayed and the remnant depleted feature might have reacted to the background zonal flow resulting in the asymmetry. Also, to our knowledge, such hemispherical asymmetry has not been reported earlier in the literature. Further, such observations might provide better insights into the later time evolution of plasma bubbles during disturbed conditions.

5. Conclusion

In this present study, EPBs were noticed to drift eastward with velocity of 30–80 m/s during 14:30–16:30 UT at different dip latitudes between 3°S and 15°N dip latitude in the Indian longitude sector. DDEF effects inferred from westward reversal of the nocturnal plasma drift were observed in this region almost 10 h after the onset of the storm main phase. DDEF effects first appeared at higher dip latitudes and subsequently extended toward the dip equator. Between 17 UT and 18:30 UT, westward drift velocity was observed to decrease and afterward it regained in magnitude again. EPBs continued to drift westward till 22 UT. On 17 March 2015, large westward tilt of EPBs was observed to map down till 3.4°N dip latitude and the maximum tilt was estimated to be few times larger than the tilts observed on the other nights during January to May 2015. Presence of latitudinal gradient in the drift velocities and occurrence of drift reversal over a relatively short period of time has been attributed as the cause of this large westward tilt.

The most interesting finding of this study was the asymmetry in tilt of the EPBs at conjugate points. To our knowledge, such asymmetry has not been reported in literature previously. Also, our study is one of the first to analyze the latitudinal behavior of the zonal drift and tilt of the EPBs during storm time from the dip equatorial region. This sort of study will strengthen our understanding of the EPB characteristics as well as variability of the equatorial ionosphere during storm time.

Acknowledgments

This work was supported by the Department of Science and Technology (DST), Government of India through Indian Institute of Geomagnetism (IIG) and through INSPIRE research grant DST/INSPIRE/04/2014/001636 to V.L.N. The airglow observations at Kolhapur were carried out through scientific collaboration between IIG and Shivaji University, Kolhapur. The lead author S. S. thanks the Director, Indian Institute of Geomagnetism for providing a research fellowship. We thank the SPDF, NASA for making the IMF B_z, *SYM-H*, *AU*, and *AL* index and *Ap* index data available in the public domain. The lead author S.S. cordially thanks his colleague Dupinder Singh for his help in performing the geographic to magnetic coordinate transformation. The ASAI data of Tirunelveli and Kolhapur are not available in the public domain. Any data related queries or data access request should be directed to S.G.

References

Anderson, D. N., and M. Mendillo (1983), Ionospheric conditions affecting the evolution of equatorial plasma depletions, *Geophys. Res. Lett.*, *10*, 541–544, doi:10.1029/GL010i007p00541.

Astafyeva, E., I. Zakharenkova, and M. Förster (2015), Ionospheric response to the 2015 St. Patrick's Day storm: A global multi-instrumental overview, *J. Geophys. Res. Space Physics*, *120*, 9023–9037, doi:10.1002/2015JA021629.

Blanc, M., and A. Richmond (1980), The ionospheric disturbance dynamo, *J. Geophys. Res.*, *85*(A4), 1669–1686, doi:10.1029/JA085iA04p01669.

Booker, H. G., and H. W. Wells (1938), Scattering of radio waves by the *F*-region of the ionosphere, *Terr. Magn. Atmos. Electr.*, *43*(3), 249–256, doi:10.1029/TE043i003p00249.

Carter, B. A., E. Yizengaw, R. Pradipta, J. M. Retterer, K. Groves, C. Valladares, R. Caton, C. Bridgwood, R. Norman, and K. Zhang (2016), Global equatorial plasma bubble occurrence during the 2015 St. Patrick's Day storm, *J. Geophys. Res. Space Physics*, *121*, 894–905, doi:10.1002/2015JA022194.

Chapagain, N. P., M. J. Taylor, and J. V. Eccles (2011), Airglow observations and modeling of *F* region depletion zonal velocities over Christmas Island, *J. Geophys. Res.*, *116*, A02301, doi:10.1029/2010JA015958.

Fejer, B. G. (1991), Low latitude electrodynamic plasma drifts: A review, *J. Geophys. Res.*, *53*(8), 671–693, doi:10.1016/0021-9169(91)90121-M.

Fejer, B. G., M. F. Larsen, and D. T. Farley (1983), Equatorial disturbance dynamo electric fields, *Geophys. Res. Lett.*, *10*, 537–540, doi:10.1029/GL010i007p00537.

Hairston, M., W. R. Coley, and R. Stoneback (2016), Responses in the polar and equatorial ionosphere to the March 2015 St. Patrick Day storm, *J. Geophys. Res. Space Physics*, *121*, 11,213–11,234, doi:10.1002/2016JA023165.

Huang, C. M., and M. Q. Chen (2008), Formation of maximum electric potential at the geomagnetic equator by the disturbance dynamo, *J. Geophys. Res.*, *113*, A03301, doi:10.1029/2007JA012843.

Huang, C.-S., G. R. Wilson, M. R. Hairston, Y. Zhang, W. Wang, and J. Liu (2016), Equatorial ionospheric plasma drifts and O+ concentration enhancements associated with disturbance dynamo during the 2015 St. Patrick's Day magnetic storm, *J. Geophys. Res. Space Physics*, *121*, 7961–7973, doi:10.1002/2016JA023072.

Kakad, B., P. Gurram, P. N. B. Tripura Sundari, and A. Bhattacharyya (2016), Structuring of intermediate scale equatorial spread *F* irregularities during intense geomagnetic storm of solar cycle 24, *J. Geophys. Res. Scape Physics*, *121*, 7001–7012, doi:10.1002/2016JA022635.
Kelley, M. C. (2009), *The Earth's Ionosphere*, pp. 131–175, Academic Press, San Diego, Calif.
Kelley, M. C., B. G. Fejer, and C. A. Gonzales (1979), An explanation for anomalous equatorial ionospheric electric fields associated with a northward turning of the interplanetary magnetic field, *Geophys. Res. Lett.*, *6*, 301–304, doi:10.1029/GL006i004p00301.
Kelley, M. C., J. J. Makela, L. J. Paxton, F. Kamalabadi, J. M. Comberiate, and H. Kil (2003), The first coordinated ground- and space-based optical observations of equatorial plasma bubbles, *Geophys. Res. Lett.*, *30*(14), 1766, doi:10.1029/2003GL017301.
Kikuchi, T., H. Lühr, T. Kitamura, O. Saka, and K. Schlegel (1996), Direct penetration of the polar electric field to the equator during a DP 2 event as detected by the auroral and equatorial magnetometer chains and the EISCAT radar, *J. Geophys. Res.*, *101*(A8), 17,161–17,173, doi:10.1029/96JA01299.
Kil, H., W. K. Lee, L. J. Paxton, M. R. Hairston, and G. Jee (2016), Equatorial broad plasma depletions associated with the evening prereversal enhancement and plasma bubbles during the 17 March 2015 storm, *J. Geophys. Res. Space Phys.*, *121*, 10,209–10,219, doi:10.1002/2016JA023335.
Makela, J. J., and M. C. Kelley (2003), Field-aligned 777.4-nm composite airglow images of equatorial plasma depletions, *Geophys. Res. Lett.*, *30*(8), 1442, doi:10.1029/2003GL017106.
Martinis, C., and M. Mendillo (2007), Equatorial spread *F*-related airglow depletions at Arecibo and conjugate observations, *J. Geophys. Res.*, *112*, A10310, doi:10.1029/2007JA012403.
Martinis, C., J. V. Eccles, J. Baumgardner, J. Manzano, and M. Mendillo (2003), Latitude dependence of zonal plasma drifts obtained from dual-site airglow observations, *J. Geophys. Res.*, *108*(A3), 1129, doi:10.1029/2002JA009462.
Mendillo, M., and J. Baumgardner (1982), Airglow characteristics of equatorial plasma depletions, *J. Geophys. Res.*, *87*(A9), 7641–7652, doi:10.1029/JA087iA09p07641.
Mendillo, M., and A. Tyler (1983), Geometry of depleted plasma regions in the equatorial ionosphere, *J. Geophys. Res.*, *88*(A7), 5778–5782, doi:10.1029/JA088iA07p05778.
Narayanan, V. L., S. Gurubaran, and K. Emperumal (2009), Imaging observations of upper mesospheric nightglow emissions from Tirunelveli (8.7°N), *Indian J. Radio Space Phys.*, *38*, 150–158.
Narayanan, V. L., S. Sau, S. Gurubaran, K. Shiokawa, N. Balan, K. Emperumal, and S. Sripathi (2014), A statistical study of satellite traces and evolution of equatorial spread *F*, *Earth Planets Space*, *66*, 160, doi:10.1186/s40623-014-0160-4.
Narayanan, V. L., S. Gurubaran, M. B. Berlin Shiny, K. Emperumald, and P. T. Patil (2017), Some new insights of the characteristics of equatorial plasma bubbles obtained from Indian region, *J. Atmos. Sol. Terr. Phys.*, *156*(2017), 80–86, doi:10.1016/j.jastp.2017.03.006.
Nava, B., J. Rodríguez-Zuluaga, K. Alazo-Cuartas, A. Kashcheyev, Y. Migoya-Orué, S. M. Radicella, C. Amory-Mazaudier, and R. Fleury (2016), Middle- and low-latitude ionosphere response to 2015 St. Patrick's Day geomagnetic storm, *J. Geophys. Res. Space Physics*, *121*, 3421–3438, doi:10.1002/2015JA022299.
Nayak, C., L.-C. Tsai, S.-Y. Su, I. A. Galkin, A. T. K. Tan, E. Nofri, and P. Jamjareegulgarn (2016), Peculiar features of the low-latitude and midlatitude ionospheric response to the St. Patrick's Day geomagnetic storm of 17 March 2015, *J. Geophys. Res. Space Physics*, *121*, 7941–7960, doi:10.1002/2016JA022489.
Nishida, A. (1968), Coherence of geomagnetic DP 2 fluctuations with interplanetary magnetic variations, *J. Geophys. Res.*, *73*, 5549–5559, doi:10.1029/JA073i017p05549.
Otsuka, Y., K. Shiokawa, T. Ogawa, and P. Wilkinson (2002), Geomagnetic conjugate observations of equatorial airglow depletions, *Geophys. Res. Lett.*, *29*(15), 1753, doi:10.1029/2002GL015347.
Patra, A. K., P. P. Chaitanya, N. Dashora, M. Sivakandan, and A. Taori (2016), Highly localized unique electrodynamics and plasma irregularities linked with the 17 March 2015 severe magnetic storm observed using multitechnique common-volume observations from Gadanki, India, *J. Geophys. Res. Space Physics*, *121*, 11,518–11,527, doi:10.1002/2016JA023384.
Pimenta, A. A., P. R. Fagundes, Y. Sahai, J. A. Bittencourt, and J. R. Abalde (2003), Equatorial *F*-region plasma depletion drifts: Latitudinal and seasonal variations, *Ann. Geophys.*, *21*, 2315–2322, doi:10.5194/angeo-21-2315-2003.
Rajesh, P. K., J. Y. Liu, H. S. S. Sinha, and S. B. Banerjee (2010), Appearance and extension of airglow depletions, *J. Geophys. Res.*, *115*, A08318, doi:10.1029/2009JA014952.
Ramsingh, S., S. Sripathi, S. Sreekumar, K. Banola, P. T. Emperumal, and B. S. Kumar (2015), Low-latitude ionosphere response to super geomagnetic storm of 17/18 March 2015: Results from a chain of ground based observations over Indian sector, *J. Geophys. Res. Space Physics*, *120*, 10,864–10,882, doi:10.1002/2015JA021509.
Rohrbaugh, R. P., W. B. Hanson, B. A. Tinsley, B. L. Cragin, J. P. McClure, and A. L. Broadfoot (1989), Images of transequatorial bubbles based on field-aligned airglow observations from Haleakala in 1984–1986, *J. Geophys. Res.*, *94*(A6), 6763–6770, doi:10.1029/JA094iA06p06763.
Sekar, R., D. Chakrabarty, and D. Pallamraju (2012), Optical signature of shear in the zonal plasma flow along with a tilted structure associated with equatorial spread *F* during a space weather event, *J. Atmos. Sol. Terr. Phys.*, *75–76*, 57–63, doi:10.1016/j.jastp.2011.05.009.
Tsunoda, R. T. (1981), Time evolution and dynamics of equatorial backscatter plumes: 1. Growth phase, *J. Geophys. Res.*, *86*(A1), 139–149, doi:10.1029/JA086iA01p00139.
Tulasi Ram, S., et al. (2016), Duskside enhancement of equatorial zonal electric field response to convection electric fields during the St. Patrick's Day storm on 17 March 2015, *J. Geophys. Res. Space Physics*, *120*, 538–548, doi:10.1002/2015JA021932.
Woodman, R. F., and C. La Hoz (1976), Radar observations of *F* region equatorial irregularities, *J. Geophys. Res.*, *81*(31), 5447–5466, doi:10.1029/JA081i031p05447.
Zalesak, S. T., S. L. Ossakow, and P. K. Chaturvedi (1982), Nonlinear equatorial spread *F*: The effect of neutral winds and background Pedersen conductivity, *J. Geophys. Res.*, *87*(A1), 151–166, doi:10.1029/JA087iA01p00151.